

Predicting PM_{2.5} Concentrations Across USA Using Machine Learning

P. Preetham Vignesh¹, Jonathan H. Jiang², P. Kishore

¹ University of California, Los Angeles, USA

² Jet Propulsion Laboratory, California Institute of Technology, Pasadena, California, USA.

³ Retired, University of California, Irvine, USA

Copyright ©2022, All Rights Reserved.

Correspondence: Jonathan.H.Jiang@jpl.nasa.gov

Keywords: Surface Temperature, Climate Model, Global Warming Projection

Abstract:

Fine particulate matter with a size less than 2.5 μm (PM_{2.5}) is increasing due to economic growth, air pollution, and forest fires in some states in the United States. Although previous studies have attempted to retrieve the spatial and temporal behavior of PM_{2.5} using aerosol remote sensing and geostatistical estimation methods the coarse resolution and accuracy limit these methods. In this paper the performance of machine learning models on predicting PM_{2.5} is assessed with Linear Regression (LR), Decision Tree (DT), Gradient Boosting Regression (GBR), AdaBoost Regression (ABR), XG Boost (XGB), k-nearest neighbors (KNN), Long Short-Term Memory (LSTM), Random Forest (RF), and support vector machine (SVM) using PM_{2.5} station data from 2017-2021. To compare the accuracy of all the nine machine learning models the coefficient of determination (R^2), root mean square error (RMSE), Nash-Sutcliffe efficiency (NSE), root mean square error ratio (RSR), and percent bias (PBIAS) were evaluated. Among all nine models the RF and SVM models were the best for predicting PM_{2.5} concentrations. Comparison of the PM_{2.5} performance metrics displayed that the models had better predictive behavior in the western United States than that in the eastern United States.

1. Introduction:

Air pollution has had negative effects on human health and has interfered with social functions; particles with diameters less than 2.5 μm (PM_{2.5}) have especially been the primary pollutants in many cities in the USA. Among air pollutants, PM_{2.5} is among the most harmful and can easily cross the human defense barrier, enter the lungs, and cause human disease and even death because of its small particle size and potential for long-term exposure (Wu et al., 2018; Chen et al., 2019c; Wei et al., 2019). The PM_{2.5} observations were from environmental monitoring stations, however, the quantity of available PM_{2.5} data presented regional differences due to the uneven station distribution.

35 He et al. (2016) conducted research that indicates the PM_{2.5} pollution index was positively correlated
36 with the emergency admission rate of female acute myocardial infarction and with the increased
37 incidence of diabetes and hypertension. According to the latest urban air quality database, 98% of
38 low and middle income countries with more than 100,000 inhabitants do not meet the World Health
39 Organization (WHO) air quality guidelines [2].

40 Several researchers have used satellite remote sensing data for spatial monitoring coverage in
41 their studies to estimate PM_{2.5} concentrations (Fang et al., 2016; Hu et al., 2017; Park et al., 2019).
42 One way of using remote sensing satellites for estimating PM_{2.5} levels is through the aerosol optical
43 depth (AOD) parameter, which refers to the solar radiation attenuation due to the scattering and
44 absorption characteristics of aerosols within the atmosphere (Hutschison et., 2005; Van Donkelaar et
45 al., 2010; Soni et al., 2018). Wang and Christopher (2003) was the first estimated PM_{2.5} using AOD
46 measurements from Moderate Resolution Imaging Spectrometer (MODIS). Several researchers noted
47 that satellite AOD as well as monitoring sources and transport of aerosols are key variables in
48 estimating PM_{2.5} and air quality (Gupta and Christopher, 2009). Most have used linear regression
49 models to correlate AOD and PM_{2.5} (Gupta and Christopher, 2009). Grahremanloo et al., 2021
50 examined seasonal behavior of PM_{2.5} over Texas using the Random Forest model. Liu et al. (2005)
51 studied PM_{2.5} levels in three different areas such as urban, suburban, and county in the Eastern United
52 States using multiple linear regression (MLR). They concluded that the model performance may
53 decrease since the satellite images have a relatively coarse spatial resolution since each pixel
54 represents a large area on the ground.

55 The design of a model for time series prediction focuses on the application of algorithms to predict
56 future events based on past trends. The model captures the variables with certain assumptions and
57 represents the existing dynamic relations, summarizing them to better understand the process that
58 produced the past data to better predict the future. Most of the above studies have used linear and

59 non-linear regressions to correlate various parameters with PM_{2.5} concentrations over a particular
60 region. In our study we focused on the entire United States and predicted PM_{2.5} concentrations over
61 various regions using different machine learning models.

62 Recently, due to an increase in the application of machine learning models to various fields
63 in order to increase the accuracy of predictions, machine learning has also been used to predict particle
64 concentrations (Kuremoto et al., 2014; Ong et al., 2016; Gui et al., 2020). However, the data mining
65 does not only differ from one study to another but also in terms of classification algorithms and used
66 features. The regression, boosting models, and deep learning-based methods display remarkable
67 performance in time-series data processing to make predictions (Hochreiter and Schmidhuber, 1997).
68 The estimation using traditional statistical methods requires a large amount of historical data to
69 construct the relationship between explanatory variables and target variables (Breiman, 2001b). Since
70 machine learning is a very promising tool to forecast pollution, we proposed applying this approach
71 to predict PM_{2.5} concentrations in the USA. The model predictions based on ML algorithms were
72 checked by cross-validation and evaluated using appropriate metrics such as root mean square
73 (RMSE) and mean absolute error (MAE).

74 Earlier studies used a limited number of statistical models, but in our study, we used nearly six
75 machine learning models to find the best accuracy of predictions. In addition to this, our research
76 paper took a novel approach in PM_{2.5} concentration research by exploring concentrations over USA
77 as opposed to China where many existing PM_{2.5} studies have already been conducted. The purpose of
78 this paper is to present the predictions of PM_{2.5} over different states over the USA. The data collection
79 and different machine learning techniques applied in the context of time series predictions are adopted
80 for the present study as described in Section 2. Results and discussion are given in Section 3 and
81 finally the overall conclusions are drawn from the present study presented in Section 4.

82 **2. Datasets:**

83 **2.1 Ground PM_{2.5} Measurements:**

84 Daily PM_{2.5} observational data was collected from January 2015 to December 2021 from the
85 openaq air quality database (<https://openaq.org/>). These datasets are available from nearly 1081
86 stations around the USA. The PM_{2.5} concentrations of ground sites were taken as the dependent
87 variable of the model. In this paper, the daily PM_{2.5} concentration data of 1081 ground monitoring
88 stations were sorted in to monthly and seasonal data from January 2015 to December 2021, and the
89 data integrity exceeded 97%. The datasets were calibrated and quality-controlled according to
90 national standards. Figure 1 shows the ground-level monitoring site coverage over the United States;
91 these sites collected 7 years of daily continuous observations. From this figure, we can see that PM_{2.5}
92 monitoring sites are greater in number in the eastern part than in the western part of USA. We
93 observed small data gaps and therefore applied linear interpolation for filling the gaps of PM_{2.5}
94 datasets. However, stations are sparsely located, therefore ground level PM_{2.5} monitoring sites face
95 difficulties in meeting the data requirements (Lin et al., 2015). As expected, the PM_{2.5} concentrations
96 were much lower at remote sites compared to urban areas, mainly due to the absence of anthropogenic
97 sources.

98 This study aims to achieve the best statistical comparison of nine machine learning models: Linear
99 Regression, K-Nearest Neighbors Regressor, Logistic Regression, Gradient Boosting Regressor, Ada
100 Boost Regressor, Decision Tree Regressor, XG Boost, Support Vector Regressor, Random Forest,
101 Support Vector Machine, and LSTM for estimating the PM_{2.5} concentrations over the specified
102 period. The datasets are split into 80% and 20% as training and testing datasets, respectively. The
103 training datasets are used to build the model, and the testing dataset is used to verify the model
104 performance of the trained model.

105 **2.2 K Nearest Neighbors (K-NN):**

106 The K-NN model is one of the earliest ML models (reference). The K-NN model categorizes each
107 unknown instance in the training set by choosing the majority class label among its k nearest
108 neighbors. Its performance is also crucially dependent on the Euclidean distance metric used to define
109 the most immediate neighbors. After determining the Euclidean distance between the data, the
110 database samples are sorted in ascending order from the least distance (maximal similarity) to
111 maximum distance (minimal similarity) [Wu et al. 2008]. The k nearest distances are looked at, and
112 the highest occurring class label of these k nearest points to the instance is decided to be the class
113 label of the previously unknown instance in the training set. Selecting an optimal value of k becomes
114 challenging since too low of a value for k can result in overfitting while a larger value of k can cause
115 the opposite to occur.

116 **2.3 Random Forest (RF):**

117 RF is a machine learning algorithm and was proposed by Breiman (2001); it integrates multiple
118 trees through the idea of ensemble learning, utilizes classification and regression tree (CART) as
119 learning algorithms of decision trees. The RF is a set of decision trees, where the structure of each
120 one, and the space of the variables is divided into smaller subspaces so that the data in each region is
121 as uniform as possible [Hastie et al., 2005 and Breiman, 2001]. It uses the bootstrap resampling
122 technique to randomly extract k samples (with replacement) from the original training set to generate
123 new training samples. RF uses multiple base classifiers to obtain higher accuracy classification results
124 by voting or averaging. RF excels because of its ability to leverage several different independent
125 decision trees in order to classify better, thereby reducing the error from using a single decision tree
126 because oftentimes viewing classification in independent directions can lead to lower error than a
127 single decision tree's direction.

128 **2.4 XGBoost:**

129 This is a highly efficient and optimized distributed gradient boosting algorithm. XGBoost
130 supports a range of different predictive modeling problems such as classification and regression. It is
131 trained by minimizing the loss of an objective function against a dataset, and the loss function is a
132 critical hyperparameter which is tied directly to the type of problem being solved. Regular gradient
133 boosting, stochastic gradient boosting, and regularized gradient boosting are the three main forms of
134 gradient boosting. For efficiency, the system features include parallelization, distributed computing,
135 out-of-core computing, cache optimization, and optimization of data structures to achieve the best
136 global minimum and run time.

137 **2.5 Long Short-Term Memory (LSTM):**

138 LSTM is well suited for prediction based on time-series data, with better performance, to learn
139 long-term dependency, and it deals with exploding and vanishing gradient problems [Alahi et al.,
140 2016, Kong et al., 2017]. LSTM is superior to traditional ML methods in processing large input data
141 and is a type of Recurrent Neural Network (RNN) [Rumelhart et al., 1986], that has been proposed
142 to predict future outputs using past inputs. LSTM is great at processing time-series data because the
143 PM_{2.5} concentrations are time-dependent, and it can better predict future air pollution concentrations
144 by learning features contained in past air pollution concentration time-series data.

145 **2.6 Decision Tree (DT):**

146 Decision Trees are one of the most commonly used machine learning models in classification and
147 regression problems. To split a node into two or more sub-nodes DT uses mean squared error (MSE).
148 It is a tree structure with three types of nodes. The root node is the initial node, which may get split
149 into further nodes of the branched tree that finally leads to a terminal node (leaf node) that represents
150 the prediction or final outcome of the model. The interior nodes and branches represent features of

151 a data set and decision rules respectively. The final prediction is the average of the value of the
152 dependent variable in that particular leaf node.

153 **2.7 Gradient Boosting Regression (GBR):**

154 The type of boosting that combines simple models called weak learners into a single composite
155 model. Gradient boosting involves optimizing the loss function and a weak learner which makes
156 predictions. Generally, the gradient descent procedure is used to minimize a set of parameters, such
157 as coefficients in a regression equation or weights in a neural network. After estimating loss or error,
158 the weights are updated to minimize that error. Gradient Boosting algorithms minimize the bias error
159 of the model. The Gradient Boosting algorithm predicts the target variable using a regressor and Mean
160 Square Error (MSE) as the cost function (for regression problems) or predicts the target variable with
161 a classifier using a Log Loss cost function (for classification problems).

162 **2.8 Support Vector Regression (SVR):**

163 The SVR model is widely applied to time series prediction problems. It is a novel forecasting
164 approach, which is trained independently based on the same training data with different targets. The
165 SVR can be used with functions that are linear or non-linear (called kernel functions). The linear
166 function is used for the linear regression model and evaluates results with metrics such as Root Mean
167 Square Error (RMSE) and Mean Absolute Error (MAE) to estimate the performance of the model.

168 **2.9 AdaBoost Regressor (ABR):**

169 AdaBoost (Adaptive Boosting) is a popular technique, as it combines multiple weak classifiers to
170 build one strong classifier. The boosting approach is a class of ensembles of ML algorithms and is
171 described by Schapire (1990). Generally, the boosting approach requires a large amount of training
172 data which is not possible for many cases, and one way of mitigating this issue is by using AdaBoost
173 (Freund and Schapire, 1997). The main difference of AdaBoosting from most of the other boosting
174 approaches is in computing loss functions using relative error rather than absolute error. AdaBoost

175 regressor fits the data set and adjusts the weights according to the error rate of the current prediction,
176 and reduces the bias as well as the variance for supervised learning.

177 **2.10 Linear Regression:**

178 Linear Regression is a great statistical tool that achieves to model and predict variables by fitting
179 the predicted values to the observed values with a straight line or surface. This fitting process is
180 implemented by reducing the average perpendicular distance from the straight line/surface (which
181 are the predictions) to the observed values which oftentimes are scattered. The lower this
182 perpendicular distance, the better the line of best fit; based on this line of best fit's equation future
183 values can be predicted. In this case, the line of best fit's equation uses the $PM_{2.5}$ values as the
184 dependent and output variable whereas time is the independent variable.

185 **3.0 Results and Discussion:**

186 Before proceeding to apply machine learning models on the $PM_{2.5}$ data we will first discuss the
187 $PM_{2.5}$ concentrations monthly mean structures, a common method of data exploration to better
188 understand the data and potentially adjust hyperparameters of the models. Figure 2 shows the USA
189 monthly anomalies and quantiles for four years using daily $PM_{2.5}$ values. The monthly anomalies are
190 in percent form, so we subtracted 100 to set the average value to zero. In addition, we estimated the
191 anomaly to be positive or negative. Using anomalies we estimated the minimum, maximum values,
192 the 25%, 75% quantiles, and the interquartile ranges for each month of the entire time period, and the
193 resultant plot is shown in Figure 2. During 2018, in USA, the highest levels of $PM_{2.5}$ were observed
194 in the inland locations and they declined nearly 20% in the year 2019. In the inland areas, $PM_{2.5}$
195 concentrations are primarily influenced by the secondary particles' formation resulting from the
196 oxidation of gaseous precursors (NO_x , SO_x , and NH_3) (South Coast Air Quality Management
197 District, 2017). $PM_{2.5}$ concentrations show a drastic change before and during pandemic years. Before

198 pandemic years the PM_{2.5} concentrations are higher in the spring and summer months especially
199 towards the end of summer (August) and early fall (September) during summer years.

200 The monthly PM_{2.5} concentrations are greatest in 2018 when compared to other years. The
201 positive anomalies are observed on a higher frequency in August 2018 whereas negative anomalies
202 are observed more in September 2018. This indicates that before COVID-19 the PM_{2.5} concentrations
203 were a little higher than in other years throughout the USA. PM_{2.5} values were also higher in the
204 Eastern USA than in Western USA (Figure not shown). The decrease was moderate (in absolute and
205 relative terms) in urban areas and progressively became lower from the urban to the rural sites. From
206 our review of recent sources, primary traffic emissions are highest at traffic sites in absolute and
207 relative terms (Masiol et al., 2015; Khan et al., 2016, Pietrogrande et al., 2016). Before proceeding
208 with applying machine learning models to the data, a preliminary statistical analysis was performed
209 for each state's PM_{2.5} values and all time series values were freed of trend and outliers. This was done
210 because otherwise the time-series data values would give rise to several issues during training like
211 overfitting or significantly decreasing the performance of the model. The seasonal and annual
212 variations were removed from all states' time series data points from the entire time period. This
213 ensured stationarity in the time series data, which is a preprocessing prerequisite before applying
214 different machine learning algorithms. This is because it is better to observe statistical properties of
215 a time series which do not change over time, since statistical properties would have to be averaged
216 for the entire time period, which is not as accurate.

217 **3.1 Evaluation Parameters:**

218 For model evaluation, the errors between the estimated and true values were evaluated using
219 several evaluation indices (Chadalawada & Babovic 2017; Shahid et al., 2018; Yi et al., 2019). The
220 statistical metrics selected for comparing the performance of the models and error-values between
221 computed and observed data are evaluated by Root Mean Square Error (RMSE): square root of the

222 mean squared differences between observed and predicted, and suggests the dispersion of the sample.
 223 Smaller RMSE indicates better performance, and as performance decreases, the RMSE increases.
 224 The coefficient of determination (R^2) indicates the collinearity (relationship) between the observed
 225 and predicted data. The R^2 value ranges from 0 to 1 (Santhi et al., 2001 and Van Liew et al., 2003).
 226 Mean absolute error (MAE): average of the absolute differences between the observed and predicted
 227 values where a small value of MAE indicates better performance. Mean absolute percentage error
 228 (MAPE): this index indicates the ratio between errors and observations, the lower the MAPE the
 229 higher the accuracy (Chen et al., 2018). Root mean square error ratio (RSR): the ratio of the RMSE
 230 to the standard deviation of measured data (Stajkowski et al., 2020). RSR is classified into four
 231 intervals: very good ($0.0 \leq RSR \leq 0.50$), good ($0.50 < RSR \leq 0.60$), acceptable ($0.60 < RSR \leq 0.70$),
 232 and unacceptable ($RSR > 0.70$), respectively (Khosravi et al., 2018). Nash-Sutcliffe efficiency (NSE):
 233 is a normalized statistical metric to determine the relative magnitude of the residual variance relative
 234 to the variance or noise (Nash and Sutcliffe 1970). NSE performance ratings are very good ($0.75 <$
 235 $NSE \leq 1.0$), good ($0.65 < NSE \leq 0.75$), satisfactory ($0.50 < NSE \leq 0.65$), and unsatisfactory ($NSE \leq$
 236 0.50). Percent bias (PBIAS): it measures the average percent of the predicted value that is smaller or
 237 larger than the observed value (Malik et al., 2018; Nury et al., 2017). The PBIAS is classified into
 238 four ranges, very good ($PBIAS < \pm 10$), good ($\pm 10 \leq PBIAS < \pm 15$), satisfactory ($\pm 15 \leq PBIAS <$
 239 ± 25), and unsatisfactory ($PBIAS \geq \pm 25$).

240
$$MSE = \frac{\sum_{i=1}^n (x_{oi} - x_{pi})^2}{N}$$

241
$$MAE = \frac{1}{N} \sum_{i=1}^n |x_{oi} - x_{pi}|$$

242

243
$$R^2 = 1 - \frac{\sum_{i=1}^n (x_{oi} - x_{pi})^2}{\sum_{i=1}^n (x_{oi} - x_{mean})^2}$$

244

245

246

$$RSR = \frac{RMSE}{STDEV_{obj}} = \frac{\sqrt{\sum_{i=1}^n (x_{oi} - x_{pi})^2}}{\sqrt{\sum_{i=1}^n (x_{oi} - x_{mean})^2}}$$

247

248

249

$$PBIAS = \left| \frac{\sum_{i=1}^n (x_{oi} - x_{pi})}{\sum_{i=1}^n x_{oi}} \right| * 100$$

250

251

252

$$NORM = \sqrt{\sum_{i=1}^n (x_{oi} - x_{pi})^2}$$

253

254

255

$$MAPE = \frac{\sum_{i=1}^n \frac{|x_{oi} - x_{pi}|}{x_{oi}}}{N} * 100\%$$

256

257

$$NSE = 1 - \left[\frac{\sum_{i=1}^n (x_{oi} - x_{pi})^2}{\sum_{i=1}^n (x_{oi} - x_{mean})^2} \right]$$

258

259 where N refers to the number of data points, x_{oi} , x_{pi} are the observed and predicted daily $PM_{2.5}$

260 concentrations, respectively.

261 The nine machine learning models can describe daily variations of observed and estimated values

262 of $PM_{2.5}$ concentrations as shown in Figure 3 and Figure 4, in which the blue curve represents the

263 observed $PM_{2.5}$ concentrations, while the red curve represents the estimated $PM_{2.5}$ concentrations.

264 We generated time series plots for all states but we showed one state from the western side of the

265 USA: California (Figure 3) and another state from east USA: New York (Figure 4). All nine machine

266 learning models show that the seasonal variability of $PM_{2.5}$ concentration is lower in the spring and

267 summer and higher in autumn and winter, maybe due to atmospheric circulation of autumn and

268 winter. The $PM_{2.5}$ concentrations in the autumn and winter are less accurate because air pollution is

269 more severe than that in spring and summer. The SVM and RF models give better agreement with

270 observed $PM_{2.5}$ concentrations. However, the California $PM_{2.5}$ estimations are less accurate than

271 those of the New York because pollution is more severe due to forest fires in the summer. Sulfate

272 concentrations may reflect regional influences of PM_{2.5}; these concentrations decreased from east to
273 west but with higher amounts in California (Meng et al. 2018).

274 Figures 5 and 6 display California and New York's scatter plots of the observed vs estimated
275 daily PM_{2.5} concentrations during the period of observations using different machine learning models
276 respectively. The scatter plot of the two variables suggests a positive linear relationship between
277 them. All points on the scatter plot lie on a straight line; this indicates the differences are zero and
278 suggest a strong correlation between the observed and estimated PM_{2.5} concentrations. Tables 1 and
279 2 indicate the performance and statistical metrics as estimated for New York and California. The
280 metrics of all models in Table 1 are for New York: Random Forest with $R^2 = 0.899$, MAE = 2.122,
281 and RMSE = 3.121 has less error than the other models. The next model with the lowest error is
282 Support Vector Machine with $R^2 = 0.857$, MAE = 2.145, and RMSE = 3.125.

283 The performance of the models at different states are good at most sites, as 73% of them show an
284 $R^2 > 0.62$ and 10% show an R^2 less than 0.3. Moreover, an average RMSE less than 4.5 Mg/m³ in
285 70% of the states and more than 5 Mg/m³ in rest of the states demonstrates good performance. PM_{2.5}
286 estimations are lower and higher than observations with high and low PM_{2.5} concentration scenarios
287 respectively, indicating that estimation accuracy will decline in extreme cases in both states. Zhan et
288 al. (2017) also found similar behavior using PM_{2.5} concentration in some parts of China. This may be
289 due to the model's lack of performance caused by a smaller amount of training data, especially
290 during extreme PM_{2.5} concentrations. Ghahremanloo et al. 2021 observed PM_{2.5} levels in Texas are
291 maximal in the summer and are attributed to higher temperatures and humidity that accelerate the
292 formation of nitrate and sulfate from NO₂ and SO₂ (Lin et al., 2019). Overall, the performance of RF
293 is reasonable, with California's R^2 , RMSE, and MAE values of 0.77, 3.051 mg/m³, and 2.233 mg/m³,
294 respectively. New York's R^2 , RMSE, and MAE values were 0.899, 3.121 mg/m³, and 2.12 mg/m³,
295 respectively. Comparing California's to New York's results, we observe that the California PM_{2.5}

296 concentration values and biases were slightly higher. Overall, the average error values are slightly
297 lower in the Eastern states than in the Western states. Each state's R2, RMSE, MAE, and bias values
298 are estimated for each model and we observed RF and SVM models produce better estimates than
299 the other models. On average, the R2 of the SVM model is 5% higher than that of the RF model. The
300 biases are 15% lower in the Eastern states than in the Western states of the USA. The high sulfate
301 concentrations around Los Angeles and Long Beach may be due to the ship emissions, since these
302 two areas combined have one-fourth of all container cargo traffic in the United States
303 (<http://www.dot.ca.gov>) (Vutukuru and Dabdub, 2008). However, the PM_{2.5} estimations in the
304 autumn and winter are less accurate because air pollution is more severe than that present in the spring
305 and summer. Among the nine machine learning models, only the SVM and RF models give desirable
306 results in the mildest air pollution cases. The LSTM model performed the outperformed among all
307 models, which can neither reflect the variations of PM_{2.5} concentrations significantly nor estimate the
308 PM_{2.5} concentrations accurately.

309 A Taylor diagram can display multiple metrics in a single plot and can be used to summarize
310 the relative skill with several states' PM_{2.5} model outputs. The Taylor diagram characterizes the
311 statistical relationship between two fields (Taylor, 2001). In this paper, observed is representing the
312 values based on observations, and predicted indicates that the values were simulated by a machine
313 learning model. Figures 7 and 8 illustrate the Random Forest and Support Vector Machine of standard
314 deviation and correlation of all states of USA. Metrics of RF and SVM were computed at each state,
315 and a number was assigned to each state considered. The position of each number appearing on the
316 plot quantifies how closely model PM_{2.5} values matches with different states. Consider state 50, for
317 example and its correlation is about 0.78. The centered standard deviation difference between the
318 observed and predicted patterns is proportional to the point on the x-axis identified as observed. The
319 dotted line contours indicate the normalized standard deviation values, and it can be seen that in the

320 case of state 50 it is centered at about 1.65. Predicted patterns that agree well with observed test data
321 will lie nearest to the observed marked point. The state values lie near or on the observed dotted line,
322 and it indicates a small predicted pattern difference. Some of the state values are slightly further from
323 the observed value, it also shows that the predicted values are larger than the observed.

324 **4. Conclusion:**

325 In this paper, we present the prediction of PM_{2.5} concentrations over USA using various machine
326 learning algorithms with the goal of improving our understanding of the differences among them.
327 Machine learning algorithms are new approaches for analyzing large datasets due to the
328 computational speed and easy implementation for massive data. In this paper we studied and
329 examined nine machine learning models (Linear Regression, Decision Tree, Gradient Boost, Ada
330 Boost, XG Boost, K-Nearest Neighbors, LSTM, Random Forest, and SVM) and their performance
331 in predicting PM_{2.5} concentrations.

332 The obtained machine learning-based methods' accuracies vary in all of USA's states, but the
333 performance of RF (California: R²=0.77, NSE = 0.817, PBIAS=7.022, and RSR=0.355; New York:
334 R²=0.899, NSE=0.811, PBIAS=2.989, and RSR=0.331) and SVM (California: R²=0.71, NSE=0.897,
335 PBIAS=7.027, and RSR=0.424; New York: R²= 0.857, NSE=0.280, PBIAS=3.011, and RSR=0.338)
336 were better than the other examined methods. Moreover, it should be noted that the accuracy and
337 performance of these machine learning methods are not constant in different climates and regions.

338 Both RF and SVM models' R² scores were between 0.71 and 0.899, RMSE scores ranged between
339 3.05 to 3.714, NSE values ranged between 0.811 to 0.899, PBIAS ranged between 2.989-7.027, and
340 RSR scores ranged between 0.331-0.424 for California and New York states. These metrics revealed
341 high model reliability and performed well for both RF and SVM and larger datasets produced better
342 prediction results.

343 Our study can also contribute to limiting human health exposure risks and helping future
344 epidemiological studies of air pollution. With the improved computational efficiency, machine
345 learning models improved prediction performance and served as a better scientific tool for decision-
346 makers to make sound PM_{2.5} control policies. Real-time measurements of the chemical composition
347 of PM_{2.5} taken as regulatory air quality measurements are needed in the future.

348 Several parameters affect PM_{2.5} concentrations; in the future, it is possible to improve the
349 performance of our machine learning models with GDP per capita, urbanization data, and other
350 atmospheric parameters which would be investigated for model development. In the United States
351 more extensive ground monitoring is needed, as the total number of stations is 1000, suggesting the
352 network of stations is too sparse for a large nation (See Figure 1). This becomes much more apparent
353 in some states as also displayed in Figure 1. However, understanding the spatial and temporal
354 distribution of each region over the United States is helpful, especially over rural areas. Considering
355 these areas, a larger amount of data for these locations and other ground-based locations would
356 enhance predicting PM_{2.5} concentrations. Furthermore, the machine learning models can always be
357 updated to yield better results as new data becomes available, therefore, the expansion of sources of
358 data becomes even more important as models can be updated.

359 **Acknowledgements:** The first author (PPV) acknowledges the Jet Propulsion Laboratory (JPL) for
360 providing him the opportunity with their summer internship program. Author JHJ conducted research
361 at the Jet Propulsion Laboratory and California Institute of Technology under contract by NASA. We
362 sincerely acknowledge the open air quality group for providing PM_{2.5} station data used in this study.

363 **Data availability:** All PM_{2.5} data used for this study can be downloaded from the public website
364 <https://openaq.org>. For additional questions regarding the data sharing, please contact the
365 corresponding author at Jonathan.H.Jiang@jpl.nasa.gov.

366 **References:**

- 367 Alahi, A., K. Goel, V. Ramanathan, A. Robicquet, L. Fei-Fei, and S. Savarese, “Social LSTM:
368 Human trajectory prediction in crowded spaces”, in Proc. IEEE Conf. Comput.Vis. Pattern
369 Recognit., Jun, 2016, pp.961-971.
- 370 Breiman, L. Random Forests, Mach. Learn. 2001, 45, 5-32. <https://doi.org/1.0.1023/A:>
371 1010933404324.
- 372 Breiman, L., 2001b, Statistical modeling: the two cultures. Stat. Sci., 16 (3), 199-215,
373 <https://doi.org/10.1214/ss/1009213726>.
- 374 Chadalawada, J., and Babovic, V., 2017. Review and comparison of performance indices for
375 automatic model induction. J. of Hydroinformatics, 21, 13-31,
376 <https://doi.org/10.2166/hydro.2017.078>.
- 377 Chen, S., Li, D.C., Zhang, H.Y., Yu, D.K., Chen, R., Zhang, B., Tan, Y.F. et al., 2019c. The
378 development of a cell-based model for the assessment of carcinogenic potential upon long-term
379 PM2.5 exposure. Environ. Int. 131, <https://doi.org/10.1016/j.envint.2019.104943>.
- 380 Fang, X., Zou, B., Liu, X., Sternberg, T., Zhai, I., 2016. Satellite-based ground PM2.5
381 estimation using timely structure adaptive modeling. Rem. Sens. Environ, 186, 152-163.
- 382 Freund, Y., Schapire, R.E., 1997. A decision-theoretic generalization of on-line learning and an
383 application to boosting, J. computer and System Sciences, 55 (1), 119-139.
- 384 Ghahremanloo, M., Lops, Y., Choi, Y., Mousavinezhad, S., 2021. Impact of the COVID-19
385 outbreak on air pollution levels in East Asia. Sci. Total Environ. 142226.
- 386 Gui, K., Che, H., Zeng, Z., Wang, Y., Zhai, S., Wang, Z., Luo, M., Zhang, L., Liao, T., Zhao,
387 H., Li, L., Zheng, Y., Zhang, X., 2020. Construction of a virtual PM2.5 observation network in
388 China based on high-density surface meteorological observations using the extreme gradient
389 boosting model. Environ. Int. 141, 105801. <https://doi.org/10.1016/j.envint.2020.105801>.

390 Gupta, P., Christopher, S.A., 2009. Particulate matter air quality assessment using integrated
391 surface, satellite, and meteorological products: 2. A neural network approach. *J. Geophys. Res.*
392 *Atmosphere* 114 (D20).

393 Hastie, T.; Tibshirani, R.; Friedman, J.; Franklin, J. The elements of statistical learning: Data mining,
394 inference and prediction. *Math. Intell.* 2005, 27, 83-85.

395 He, X. N., Chen, P., Zhang, C., Chen, J.Y. Study on the correlation between PM2.5 and onset of acute
396 myocardial infarction among female patients. *Child Care China* 31, 22, 4626-4629, 2016.

397 Hu, X., Belle, J.H., Meng, X., Wildani, A., Waller, L.A., et al. Estimating PM2.5 concentrations in
398 the conterminous United States using the Random Forest approach. *Environ, Sci., Technol.* 2017,
399 51, 6936-6944. <https://doi.org.10.1021/acs.est.7b01210>.

400 Hochreiter, S., and Schmidhuber, J., 1997. Long short-term memory, *Neural Comput.*, 9, 8, 1735-
401 1780.

402 Hutschison, K.D., Smith, S., Faruqui, S.J., 2005. Correlating MODIS aerosol optical thickness data
403 with ground-based PM2.5 observations across Texas for use in a real time air-quality prediction
404 system. *Atmos. Environ.* 39 (37), 7190-7203.

405 Lin, C., Li, Y., Yuan, Z., Lau, A.K.H., Li, C., Fung, J.C.H., 2015. Using satellite remote sensing
406 data to estimate the high-resolution distribution of ground-level PM2.5. *Remote Sens. Environ.*
407 156, 117-128. <https://doi.org/10.1016/j.rse.2014.09.015>.

408 Khan, M.B., Masiol, M., Forementon, G., Gilio, A.D., de Gennaaro, G., Agostinelli, C., and
409 Pavoni, B, 2016. Carbonaceous PM2.5 and secondary organic aerosol across the Veneto region (NE
410 Italy). *Sci. Total Environ.* 542, 172-181, doi:10.1016/j.scitotenv.2015.10.103.

411 Khosravi, K ; Mao, L; Kisi, O; Yaseen, Z. M; Shahid, S. Quantifying hourly suspended sediment load
412 using data mining models: case study of a glacierized Andean catchment in Chile. *J. Hydrol.*
413 2018, 567, 165-179.

414 Kong, W., Z. Y. Dong, Y. Jia, D. J. Hill, Y. Xu, and Y. Zhang. "Short-term residential load forecasting
415 based on LSTM recurrent neural network", IEEE Trans. Smart Grid, vol. 10, no.1, pp. 841-851,
416 Jan. 2017.

417 Kuremoto, T., Kimura, S., Kobayashi, K., and Obayashi, M., 2014. Time series forecasting using a
418 deep belief network with restricted Boltzmann machines, Neurocomputing, 137, 47-56.

419 Liu, B., Philip, S. Y.; Top 10 algorithms in data mining. Knowl. Inf. Syst. 2008, 14, 1-37.

420 Liu, Y., Sarnat, J.A., Kilaru, V., Jacob, D.J., Koutrakis, P., 2005. Estimating ground-level PM2.5 in
421 the eastern United States using satellite remote sensing, Environ. Sci. Technol., 39, 3269-3278.

422 Malik, A.; Kumar. A.; Kisi, O. Daily pan evaporation estimation using heuristic methods with gamma
423 test. J. Irrig. Drain. Eng. 2018, 144, 4018023.

424 Masiol, M., Benetello, F., Harrisom, R.M., Fornenton, G., Gaspari, F.D., and Pavoni, B., 2015.
425 Spatial, seasonal trends and trans-boundary transport of PM2.5 inorganic ions in the Veneto
426 region (northeastern Italy), Atmos. Environ., 117, 19-31, doi:10.1016/j.atmosenv.2015.06.044.

427 Meng, X., Garay, M.J., Diner, D.J., Kalashnikova, O.V., Xu, J., Liu, Y., 2018. Estimating PM2.5
428 speciation concentrations using prototype 4.4 km resolution misr aerosol properties over Southern
429 California, Atmos. Environ., 181, 70-81.

430 Nash J. E., Sutcliffe, J. V. River flow forecasting through conceptual models part I – A discussion of
431 principles. J. Hydrol. 1970, 10, 282-290.

432 Nury, A.H.; Hasan, K.; Alam, M. J. Bin comparative study of wavelet-ARIMA and wavelet-ANN
433 models for temperature time series data in northeastern Bangladesh. J. King. Saud. Univ. Sci.
434 2017, 29, 47-61.

435 Ong, B.T., Sugiura, K., and Zettsu, K., 2016. Dynamically pre-trained deep recurrent neural networks
436 using environmental monitoring for predicting PM2.5, Neural Comput. Appl., 27, 6, 1553-1566.

437 Park, Y., Kwon, B., Heo, J., Hu, X., Liu, Y., Moon, T. 2019. Estimating PM2.5 concentration of the
438 conterminous Unites states via interpretable convolucional neural networks. Environ. Pollut.
439 113395.

440 Pietrogrande, M.C., Bacco, D., Ferrari, S., Ricciardelli, I., Scotto, F., Trentini, A., and Visentin, M.:
441 2016. Characteristics and major sources of carbonaceous aerosols in PM2.5 in Emilia Romagna
442 Region (Northern Italy) from four-year observations. Sci. Total Environ., 553, 172-183,
443 doi:10.1016/j.scitotenv.2016.02.074.

444 Santhi, C; Arnold, J. G.; Williams, J. R.; Dugas, W. A; Srinivasan, R.; and Hauck, L. M. Validation
445 of the swat model on a large river basin with point and non-point sources, JAWRA. J. Am. Water
446 Resour. Assoc., 2001, 37, 1169-1188.

447 Schapire, R. (1990). The strength of weak learnability. Machine Learning, 5 (2), 197-227.

448 Freund, Y., Schpire, R (1997). A decision-theoretic generalisation of on-line learning and an
449 application of boosting. J. Computer and System Sciences, 55 (1), 119-139.

450 Soni, M., Payra, S., Verma, S., 2018. Particulate matter estimation over a semi-arid region Jaipur,
451 India using satellite AOD and meteorological parameters. Atmospheric Pollution Research 9 (5),
452 949-958.

453 Stajkowski, S; Kumar, D; Samui, P; Bonakdari, H; and Gharabaghi, B, Genetic algorithm-optimized
454 sequential model for water temperature prediction, Sustainability, 12, 13, 5374, 2020.

455 Rumelhart, D. E., G. E. Hinton, and R. J. Williams, “learning representations by back-propagating
456 errors, “Nature, Vol. 323, no.6088, pp. 533-536, 1986.

457 Taylor, K.E., Summarizing multiple aspects of model performance in a single diagram, J. Geophys.
458 Res., 106, 7183-7192, 2001.

459 Van Donkelaar, A., Martin, R.V., Brauer, M., Kahn, R., Levy, R., Verduzco, C., Villeneuve, P.J.,
460 2010. Global estimates of ambient fine particulate matter concentrations from satellite-based
461 optical depth: development and application. *Environ. Health Perspect.* 118 (6), 847-855.

462 Van Liew, M. W; Arnold, J. G.; Garbrecht, J. D. Hydrologic simulation on agricultural watersheds:
463 Choosing between two models. *Trans. ASAE* 2003, 56, 1539.

464 Vutukuru, S., Dabdub, D., 2008. Modeling the effects of ship emissions on coastal air quality: a case
465 study of Southern California. *Atmos. Environ.* 42, 3751-3764.

466 Wang, J., Christopher, S.A., 2003. Intercomparison between satellite-derived aerosol optical
467 thickness and PM_{2.5} mass: Implications for air quality studies. *Geophys. Res. Lett.* 30 (21).

468 Wei, J., Huang, W., Li, Z., Xue, W., Peng, Y., Sun, L., Gribb, M., 2019. Estimating 1-km resolution
469 PM_{2.5} concentrations across China using space-time random forest approach. *Rem. Sens.*
470 *Environ.* 231, 111221.

471 World Health Organization, media centre (2016). Air pollution levels are rising in many of the
472 world's poorest cities: <http://www.int/mediacentre/news/releases/2016/air-pollution-raising/>.

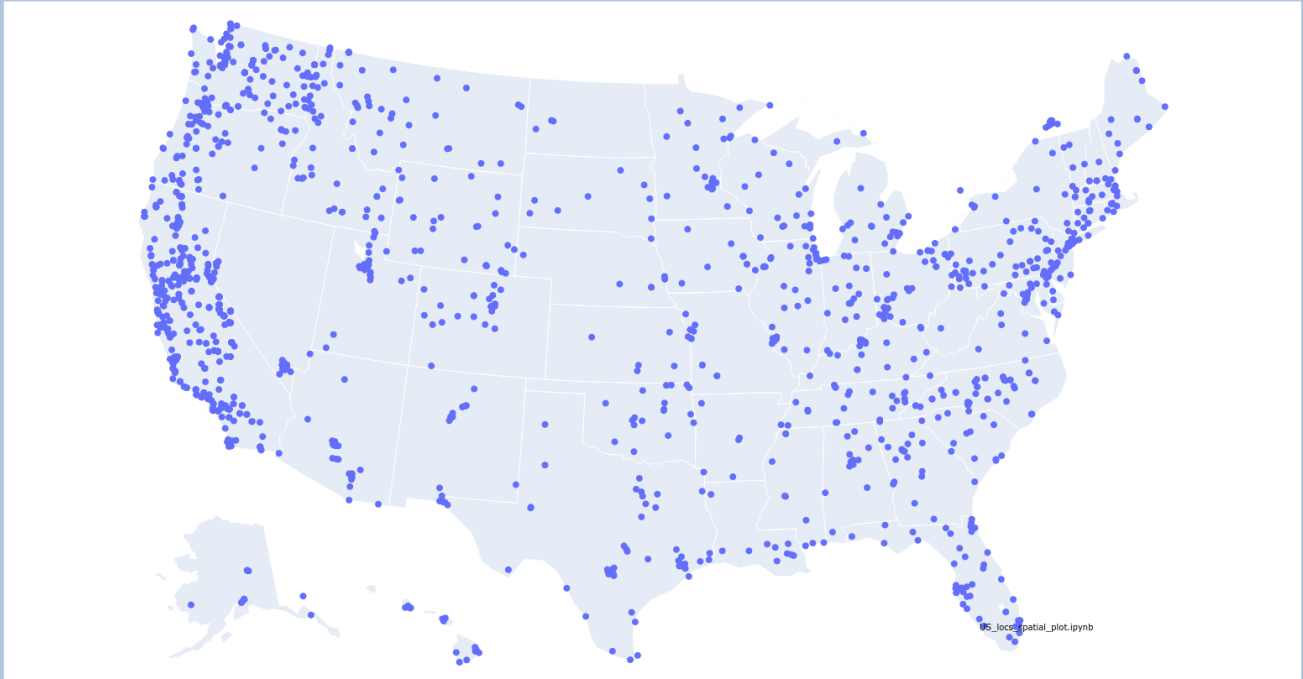
473 Wu, X.; Kumar, V.; Quinlan, J. R.; Ghosh, J.; Yang, Q.; Motoda, H.; McLachlan, G. J.; Ng, A.;

474 Yi. L., Mengfan, T., Kun, Y., Yu, Z., Xiaolu, Z., Miao, Z., Yan, S., 2019. Research on PM_{2.5}
475 estimation and prediction method and changing characteristics analysis under long temporal and
476 large spatial scale – a case study in China typical regions. *Sci. Total Environ.* 696, 133983,
477 <https://doi.org/10.1016/j.scitotenv.2019.133983>.

478 Zhang, Y., Cao, F., 2015. Fine particle matter (PM_{2.5}) in China at a city level. *Sci. Rep.*, 5, 14884.

479

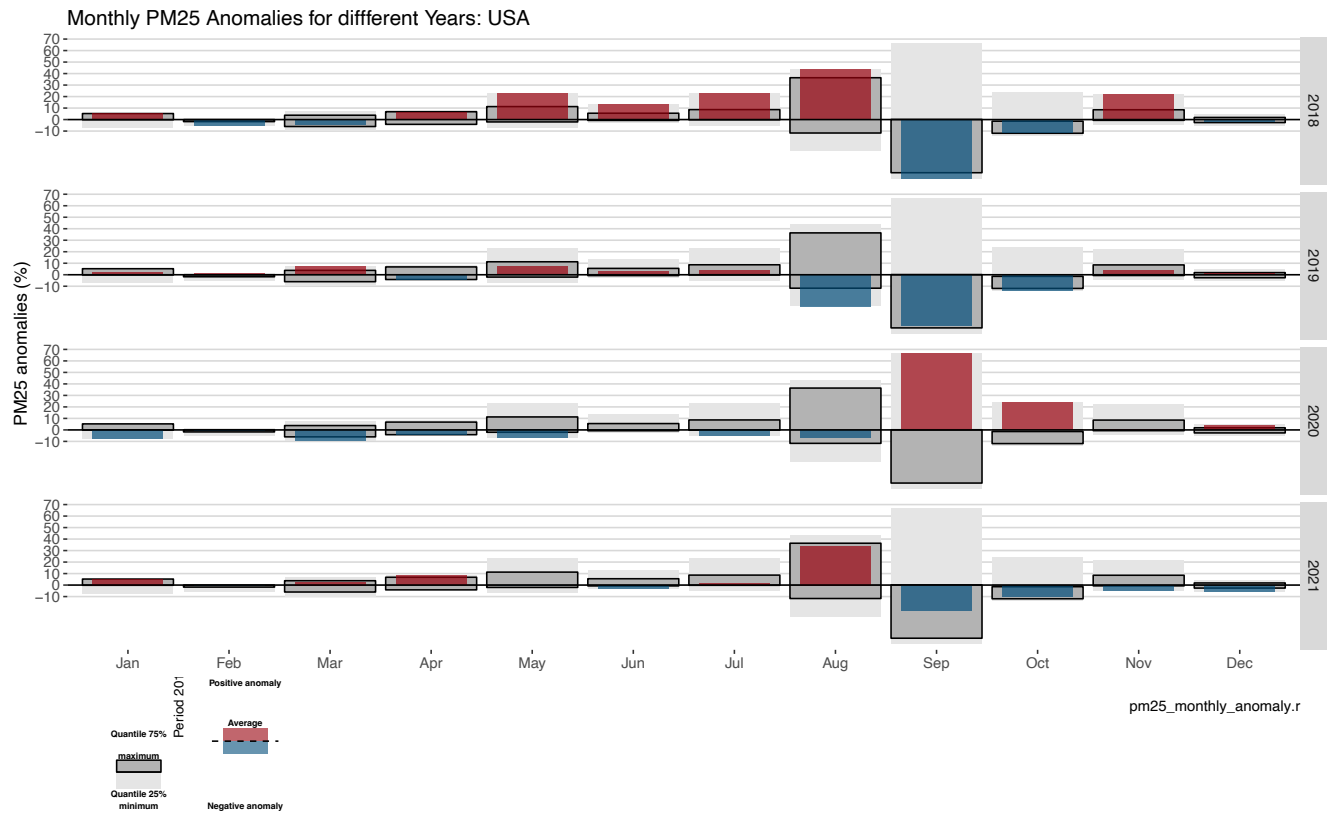
PM2.5 Locations
Locations: 1691



480

481

Figure 1. Locations of PM_{2.5} monitoring sites over USA



482

483 **Figure 2.** Monthly anomalies and quantiles for the observed period (2018-2021) using daily PM_{2.5}

484 values over United States.

485

486

487

488

489

490

491

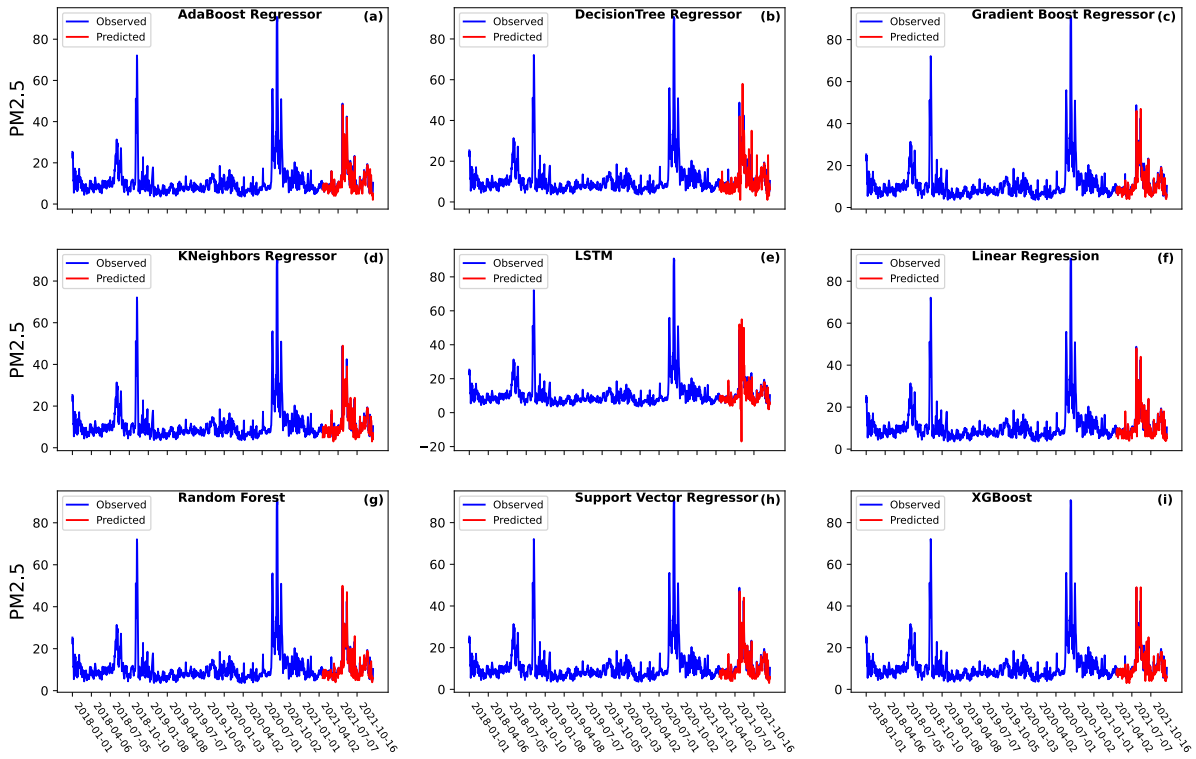
492

493

494

495

496



PM25_dly_dfrntmdl_obs_pred_lineplt.ipynb

497

498

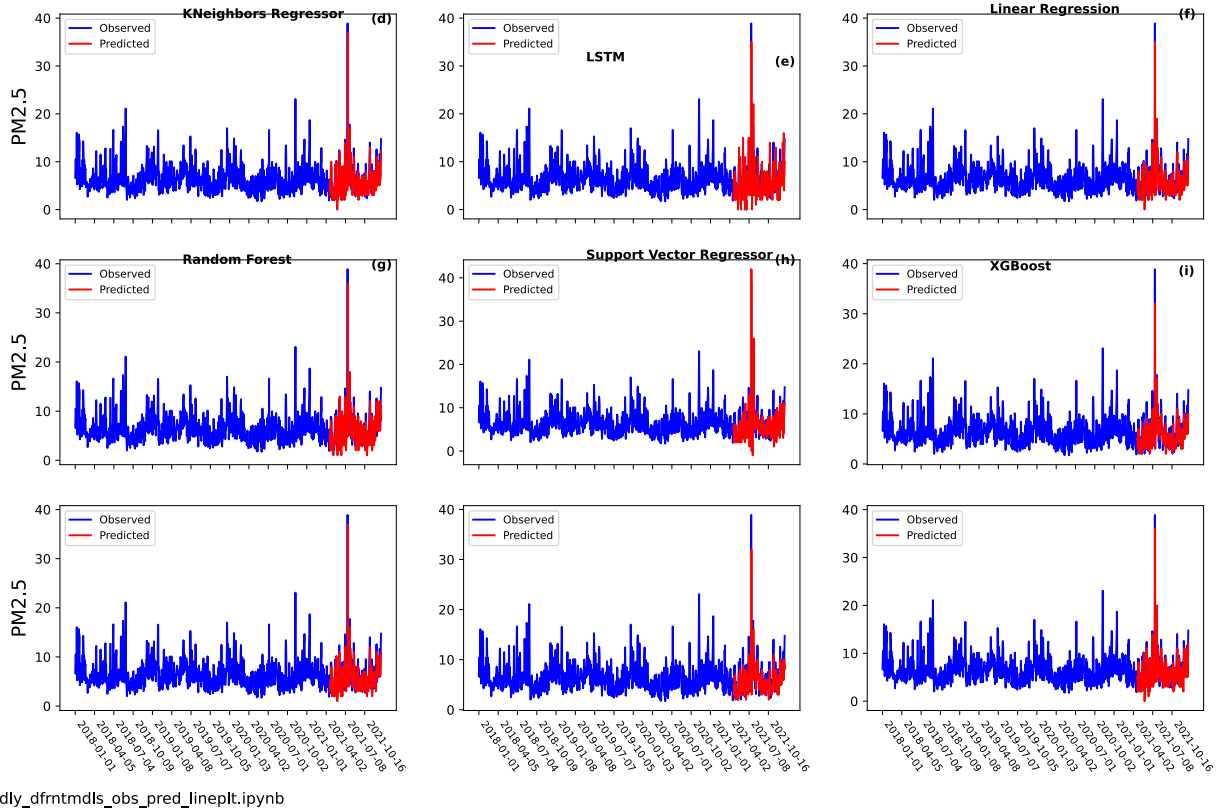
499

500

501

502

Figure 3. The comparison of the time series of estimated and observed $PM_{2.5}$ concentrations over California using different machine learning models: (a) AdaBoost regressor, (b) Decision Tree regression, (c) Gradient Boost regression, (d) K-neighbors regression (e) LSTM, (f) Linear regression, (g) Random Forest, (h) Support Vector regression, and (I) XGBoost.

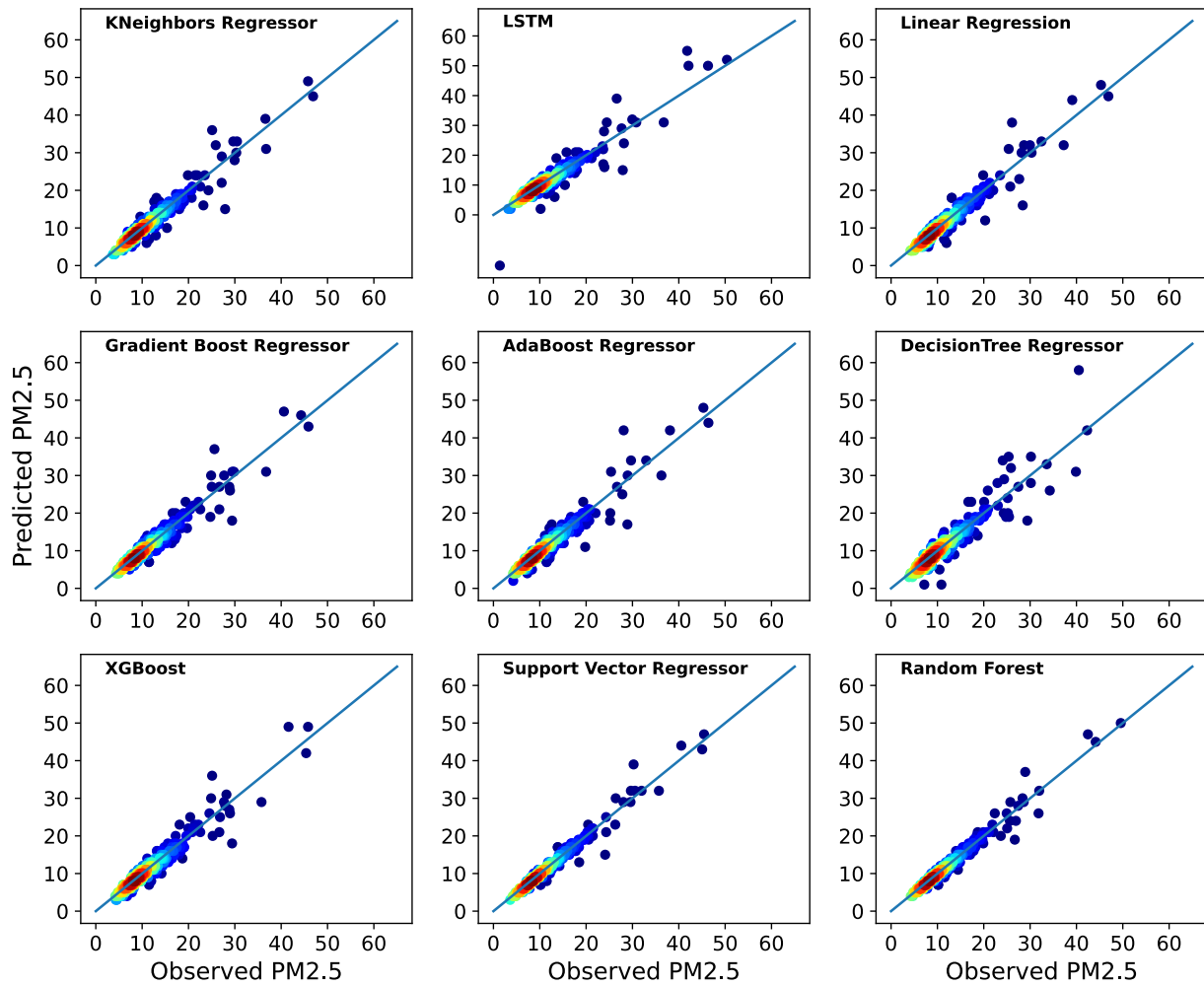


503

504 **Figure 4.** The comparison of the time series of estimated and observed $PM_{2.5}$ concentrations over
 505 New York using different machine learning models: (a) AdaBoost regressor, (b) DecisionTree
 506 regression, (c) Gradient Boost regression, (d) Kneighbors regression (e) LSTM, (f) Linear regression,
 507 (g) Random Forest, (h) Support Vector regression, and (I) XGBoost.

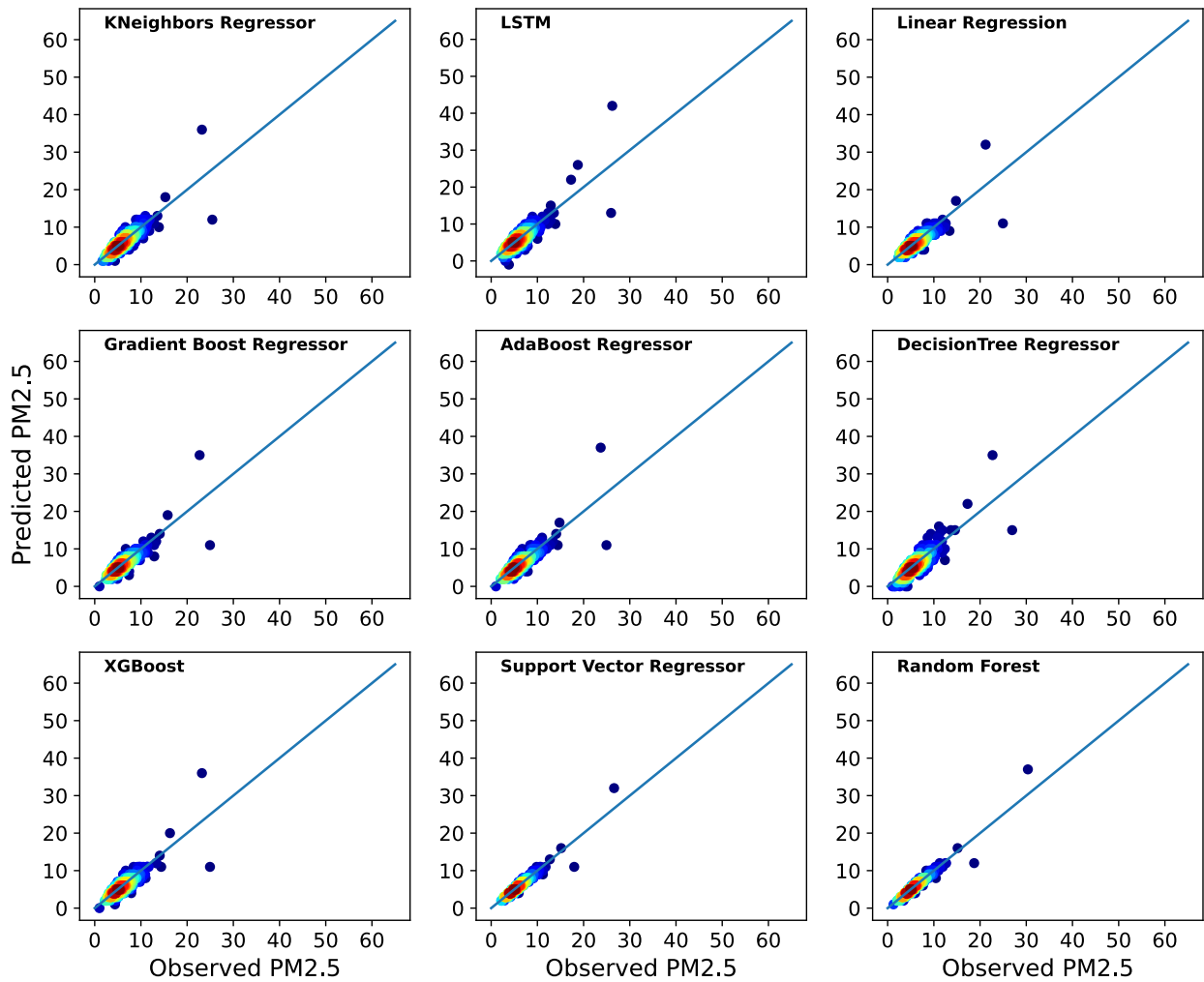
508

509



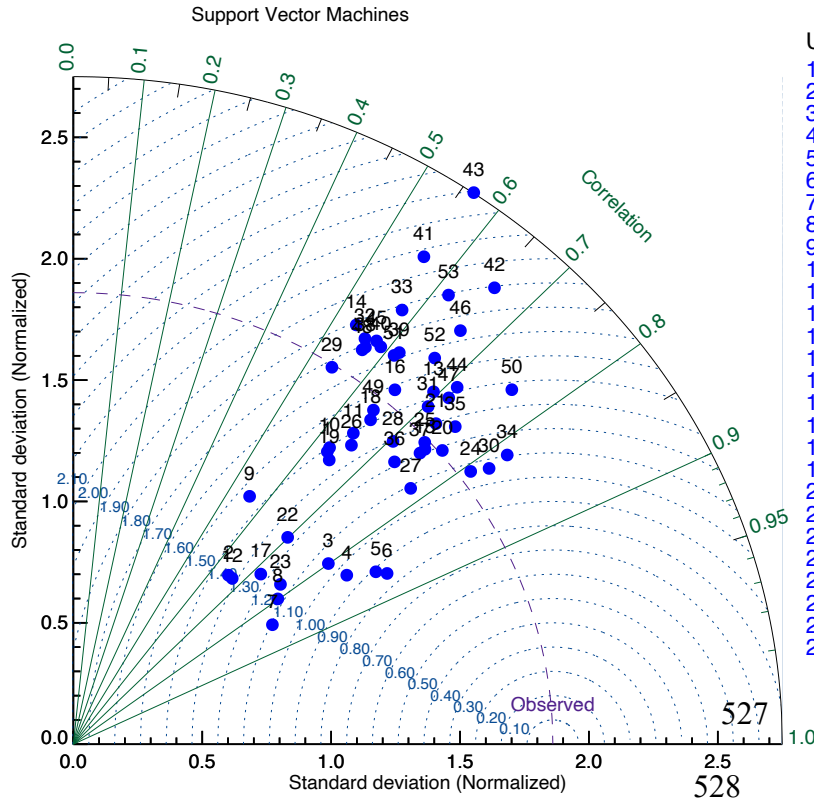
510

511 **Figure 5.** Scatter plots of observed and estimated daily PM_{2.5} concentrations over California using
 512 different machine learning models: (a) AdaBoost regressor, (b) DecisionTree regression, (c) Gradient
 513 Boost regression, (d) Kneighbors regression (e) LSTM, (f) Linear regression, (g) Random Forest, (h)
 514 Support Vector regression, and (I) XGBoost.
 515



516

517 **Figure 6.** Scatter plots of observed and estimated daily PM_{2.5} concentrations over New York using
 518 different machine learning models: (a) AdaBoost regressor, (b) DecisionTree regression, (c) Gradient
 519 Boost regression, (d) Kneighbors regression (e) LSTM, (f) Linear regression, (g) Random Forest,
 520 (h) Support Vector regression, and (I) XGBoost.



USA states

- 1:Alaska
- 2:Alabama
- 3:Arkansas
- 4:Arizona
- 5:California
- 6:Colorado
- 7:Connecticut
- 8:District of Columbia
- 9:Delaware
- 10:Florida
- 11:Georgia
- 12:Hawaii
- 13:Iowa
- 14:Idaho
- 15:Illinois
- 16:Indiana
- 17:Kansas
- 18:Kentucky
- 19:Louisiana
- 20:Massachusetts
- 21:Maryland
- 22:Maine
- 23:Michigan
- 24:Minnesota
- 25:Missouri
- 26:Mississippi
- 27:Montana
- 28:North Carolina
- 29:North Dakota
- 30:Nebraska
- 31:New Hampshire
- 32:New Jersey
- 33:New Mexico
- 34:Nevada
- 35:New York
- 36:Ohio
- 37:Oklahoma
- 38:Oregon
- 39:Pennsylvania
- 40:Puerto Rico
- 41:Rhode Island
- 42:South Carolina
- 43:South Dakota
- 44:Tennessee
- 45:Texas
- 46:Utah
- 47:Virginia
- 48:Vermont
- 49:Washington
- 50:Wisconsin
- 51:West Virginia
- 52:Wyoming

522

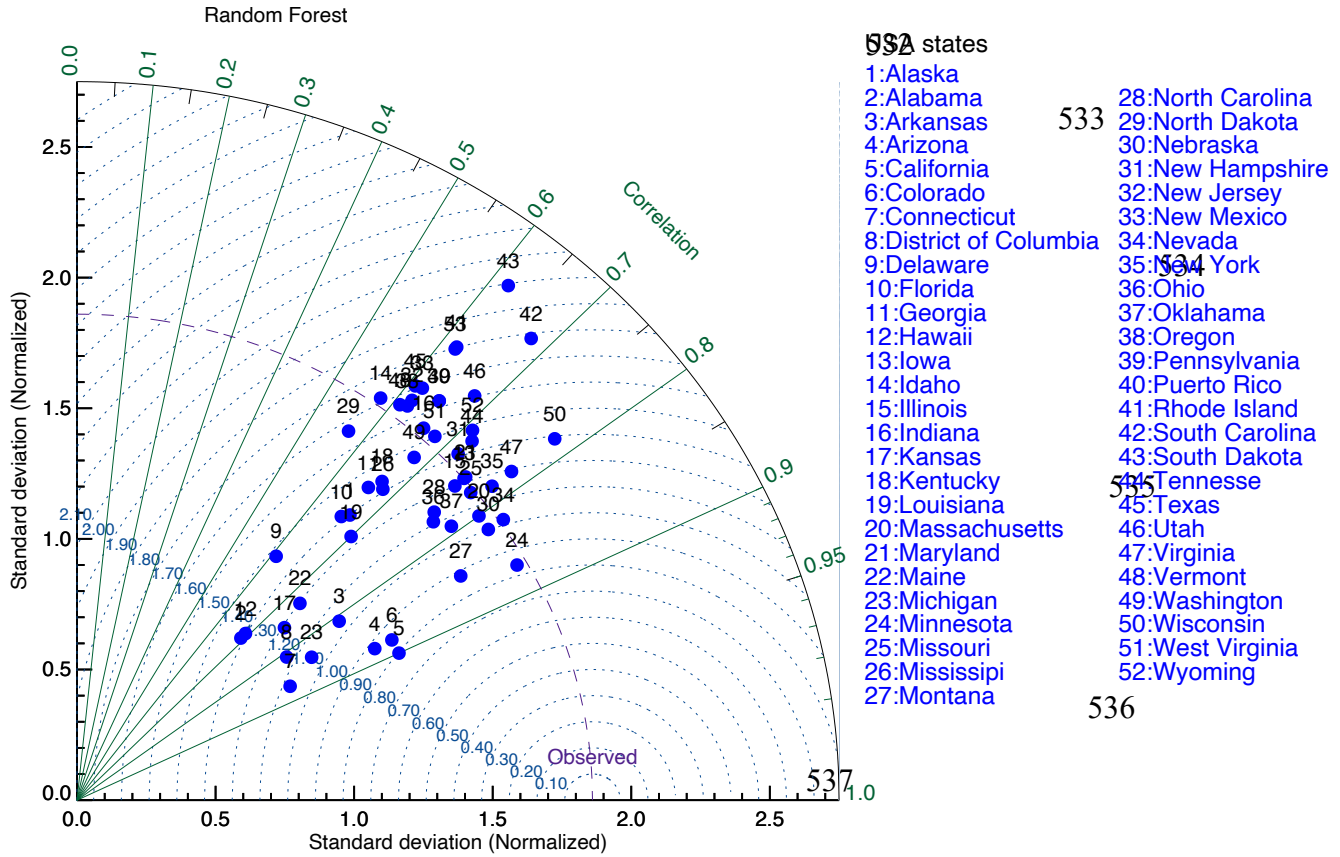
526

527
528

taylor_pm25mod.pro

529

530 **Figure 7.** Taylor diagram of the Support Vector Machines (SVM) over each state of the United States.



- USA states
- 1:Alaska
 - 2:Alabama
 - 3:Arkansas
 - 4:Arizona
 - 5:California
 - 6:Colorado
 - 7:Connecticut
 - 8:District of Columbia
 - 9:Delaware
 - 10:Florida
 - 11:Georgia
 - 12:Hawaii
 - 13:Iowa
 - 14:Idaho
 - 15:Illinois
 - 16:Indiana
 - 17:Kansas
 - 18:Kentucky
 - 19:Louisiana
 - 20:Massachusetts
 - 21:Maryland
 - 22:Maine
 - 23:Michigan
 - 24:Minnesota
 - 25:Missouri
 - 26:Mississippi
 - 27:Montana
 - 28:North Carolina
 - 29:North Dakota
 - 30:Nebraska
 - 31:New Hampshire
 - 32:New Jersey
 - 33:New Mexico
 - 34:Nevada
 - 35:New York
 - 36:Ohio
 - 37:Oklahoma
 - 38:Oregon
 - 39:Pennsylvania
 - 40:Puerto Rico
 - 41:Rhode Island
 - 42:South Carolina
 - 43:South Dakota
 - 44:Tennessee
 - 45:Texas
 - 46:Utah
 - 47:Virginia
 - 48:Vermont
 - 49:Washington
 - 50:Wisconsin
 - 51:West Virginia
 - 52:Wyoming

taylor_pm25.pro

539

540 **Figure 8.** Taylor diagram of the Random Forest (RF) over each state of the United States.

541 **Table 1:** Different Model Metrics for New York State

| New York | | | | | | | | |
|---------------------------------|-------|-------|-------|-------|-------|---------|-------|-------|
| Model | RMSE | MAE | MAPE | R2 | NSE | NORM | PBIAS | RSR |
| Linear Regression | 3.883 | 2.309 | 0.285 | 0.688 | 0.613 | 60.156 | 11.24 | 0.561 |
| Decision Tree | 5.136 | 3.109 | 0.254 | 0.454 | 0.533 | 79.58 | 13.44 | 0.691 |
| Gradient Boost Regressor | 3.822 | 2.394 | 0.545 | 0.698 | 0.683 | 59.207 | 8.210 | 0.546 |
| AdaBoost Regressor | 3.961 | 2.316 | 0.188 | 0.676 | 0.683 | 61.369 | 9.653 | 0.576 |
| XG Boost | 3.898 | 2.501 | 0.202 | 0.686 | 0.681 | 60.393 | 8.342 | 0.559 |
| KNeighbors Regressor | 3.919 | 2.379 | 0.195 | 0.683 | 0.677 | 60.711 | 7.515 | 0.562 |
| LSTM | 7.487 | 3.359 | 0.218 | 0.158 | 0.455 | 115.991 | 6.020 | 0.812 |
| Random Forest | 3.121 | 2.122 | 0.182 | 0.899 | 0.811 | 38.671 | 2.989 | 0.331 |
| SVM | 3.125 | 2.145 | 0.183 | 0.857 | 0.820 | 39.161 | 3.011 | 0.338 |

542
 543 RMSE = Root mean squared error
 544 MAE = Mean absolute error

545 MAPE = Mean absolute percentage error
 546 R^2 = The coefficient of determination
 547 NSE = Nash-Sutcliffe efficiency
 548 PBIAS = Percent Bias
 549 RSR = root mean square error ratio

550
 551

552 **Table 2:** Different Model Metrics for California State

| California | | | | | | | | |
|---------------------------------|-------|-------|-------|-------|-------|--------|--------|-------|
| Model | RMSE | MAE | MAPE | R^2 | NSE | NORM | PBIAS | RSR |
| Linear Regression | 3.695 | 2.599 | 0.326 | 0.43 | 0.694 | 57.243 | 12.086 | 0.932 |
| Decision Tree | 5.481 | 3.743 | 0.467 | 0.23 | 0.576 | 84.917 | 19.901 | 0.732 |
| Gradient Boost Regressor | 4.051 | 2.736 | 0.340 | 0.28 | 0.461 | 62.758 | 16.891 | 1.017 |
| AdaBoost Regressor | 3.804 | 2.636 | 0.342 | 0.33 | 0.435 | 58.938 | 17.532 | 0.969 |
| XG Boost | 4.271 | 2.972 | 0.372 | 0.17 | 0.438 | 66.178 | 18.726 | 1.075 |
| KNeighbors Regressor | 4.394 | 3.062 | 0.392 | 0.22 | 0.286 | 68.071 | 17.076 | 1.106 |
| LSTM | 5.025 | 3.252 | 0.339 | 0.46 | 0.309 | 77.853 | 18.027 | 0.618 |
| Random Forest | 3.051 | 2.233 | 0.315 | 0.77 | 0.817 | 46.894 | 7.022 | 0.355 |
| SVM | 3.714 | 2.618 | 0.320 | 0.71 | 0.897 | 47.853 | 7.027 | 0.424 |

553
 554 RMSE = Root mean squared error
 555 MAE = Mean absolute error
 556 MAPE = Mean absolute percentage error
 557 R^2 = The coefficient of determination
 558 NSE = Nash-Sutcliffe efficiency
 559 PBIAS = Percent Bias
 560 RSR = root mean square error ratio

561